Supporting Information

Controlled electrochemical doping of graphene-based 3D nanoarchitectures electrodes for supercapacitors and capacitive deionization

A. M. Abdelkader,[a] and D. J. Fray[b]

[a] *National Graphene Institute (NGI), University of Manchester, Booth Street East, Manchester, M13 9QS, UK. Now at Cambridge Graphene Centre, University of Cambridge, 9JJ Thomson Avenue, Cambridge, CB3 0FA, UK*

[b] *Department of Materials Science and Metallurgy, University of Cambridge, 27 Charles Babbage Road, Cambridge, CB3 0FS, UK*

Calculating the electrosorption capacity

The electrosorption capacity (Q) of the electrode was calculated from the following equation:

$$Q = \frac{(C0 - Cav)\,V}{M}$$

Where C_0 (mg L^{-1}) is the initial influent NaCl concentration, C_{av} is the equilibrium concentration salt concentration, V (L) is the total volume NaCl solution during the charging step, and M (g) represents the total mass loading of the active material in the electrode.

The charge efficiency Λ was calculated from the equation:

$$\Lambda = Q/\Sigma$$

$$\Sigma = \int I\,dt$$

Where Q is the electrosorption capacity calculated at equilibrium (at the point of minimum conductivity in the outlet stream and Σ (C g^{-1}) is the equilibrium charge, calculated by integration of the corresponding current with time.

Calculating the specific capacitance obtained from CV and charge-discharge curves

The specific capacitances (C) were computed from the charge-discharge curves using the following equation:

$$C = 4I\Delta t / m\Delta V$$

Where *I* is the constant charge current, *t* is the time of the discharging, *m* is the mass of the active material in the electrode, *V* is the voltage of capacitor after constant current charging.

From CV curves, the specific capacitances were calculated according to the following equation:

$$C = (\int IdV)/(vmV)$$

Where v is the potential scanning rate.

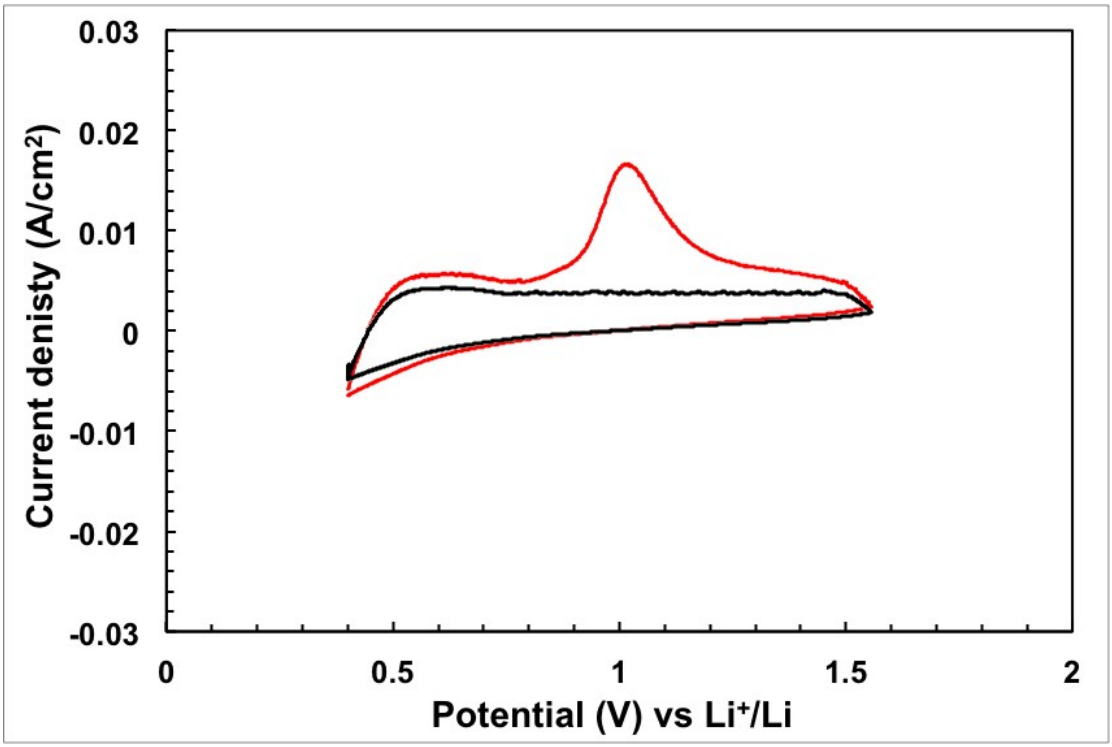

Figure S1: Cyclic voltammogram of GO electrode measured in molten KCl-LiCl-Li_3N (red) and molten KCl-LiCl (black) showing clear oxidation peak in the presence of nitrogen ions.

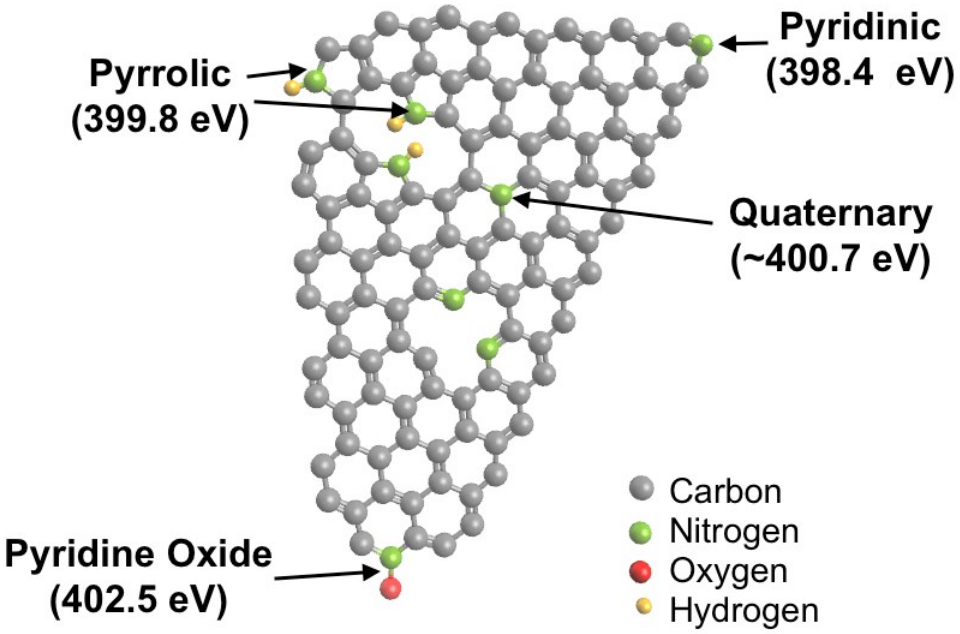

Figure S2: a schematic illustration of the various N-containing groups in graphene.

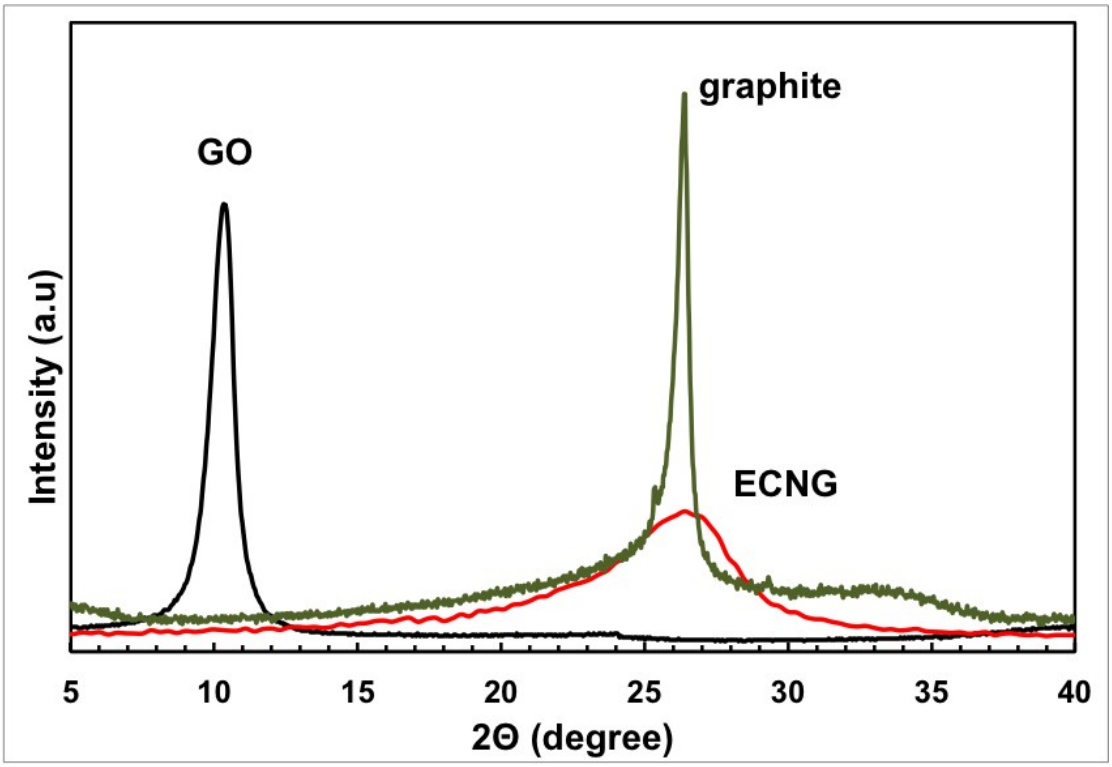

Figure S3: XRD pattern of the GO, ECNG, and graphite.

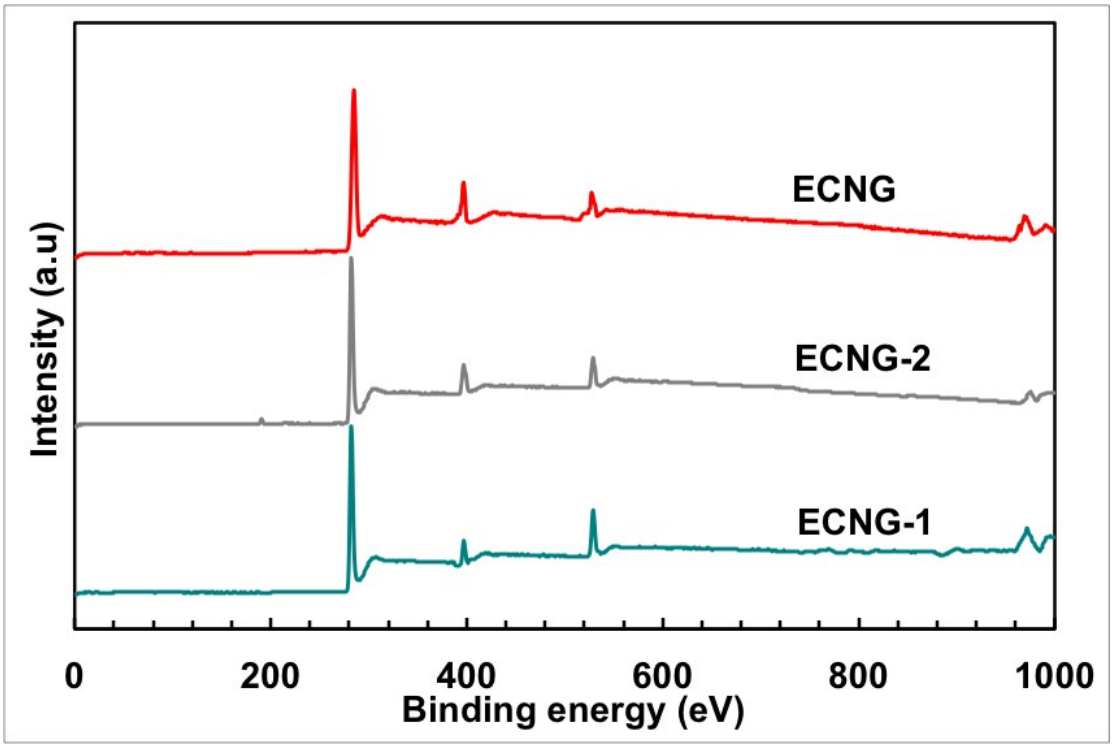

Figure S4: XPS scan of the electrochemically treated graphene after different electrolysis time.

Table S1: Electrolysis condition and the surface elemental compositions in the electrochemically treated graphene oxide estimated from the XPS spectra

Sample	Time of Electrolysis (hours)	Applied voltage (V)	Electrolyte	N at. %	O at. %
ECNG-1	1	2.5	KCl-LiCl-Li_3N	2.1	9.3
ECNG-2	2	2.5	KCl-LiCl-Li_3N	4.2	5.8
ECNG	3	2.5	KCl-LiCl-Li_3N	7.4	4.9
Undoped	3	2.5	KCl-LiCl	0	4.7
V2-ECNG	3	2.0	KCl-LiCl-Li_3N	5.3	6.9
V3-ECNG	3	3.5	KCl-LiCl-Li_3N	0.8	3.6

It is worth noting from this table that even after short electrolysis time (one hour for the ECNG-1) the oxygen content dropped one third of its value in GO and the nitrogen doping was as high as 2.1%, indicating the fast kinetic of the electrochemical reduction and doping.

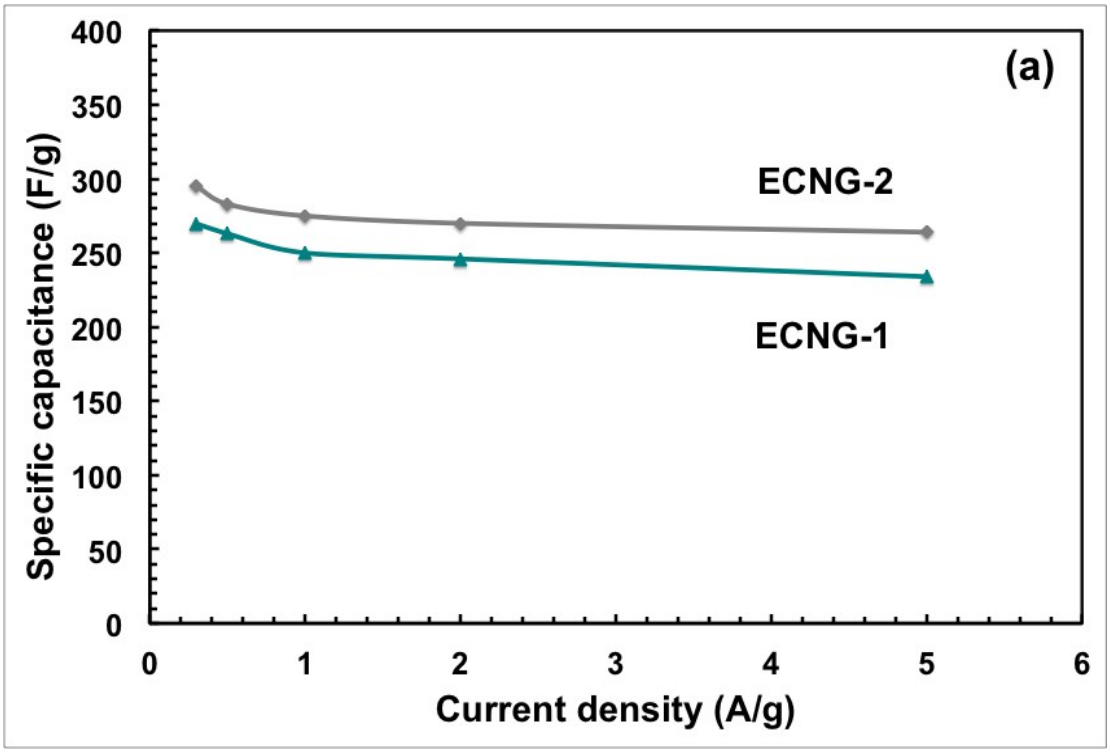

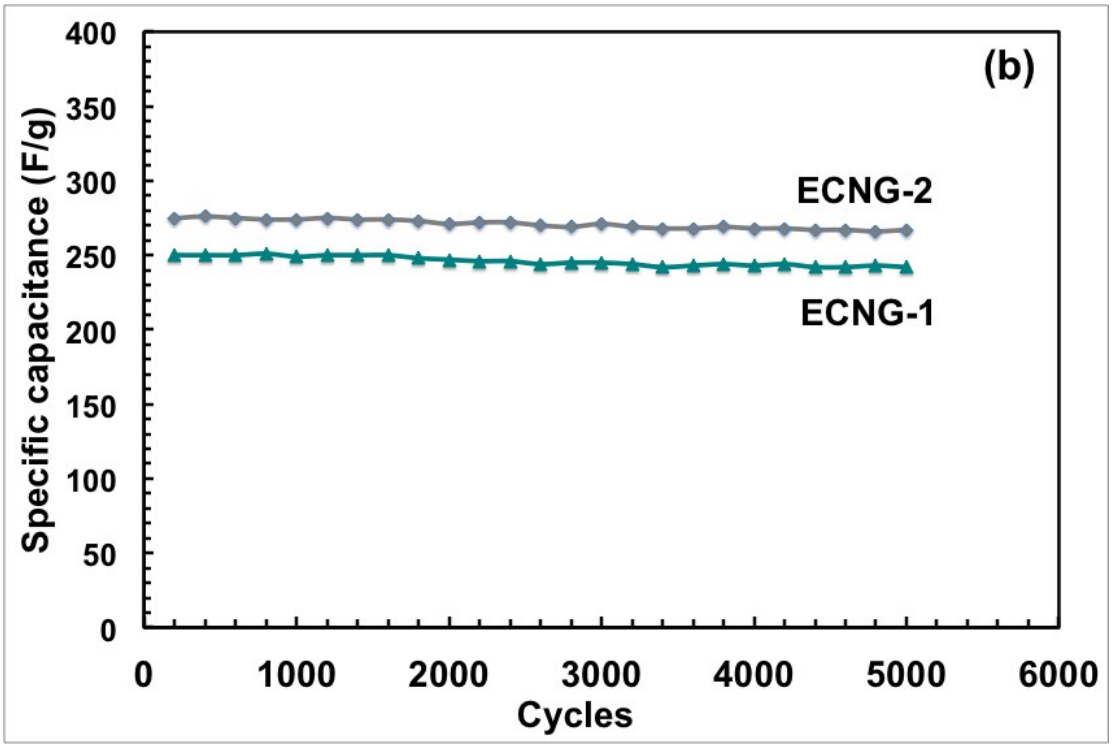

Figure S5: The electrochemical performance of the supercapacitor symmetrical devices made of ECNG-1 and ECNG-2 electrodes measured in 6 M KOH solution. The specific capacitance measured at different current density from the (a) and the cyclic performance of the charge/discharge curve and (b) cycle life measured at 1 A g^{-1}

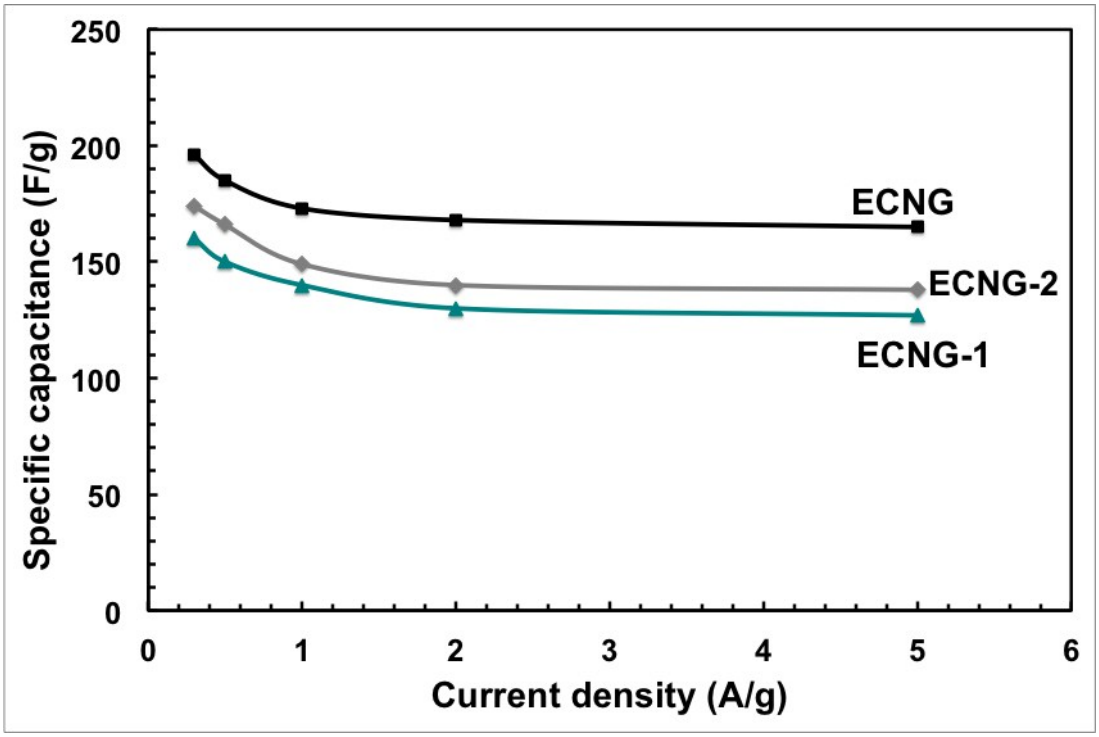

Figure S6: The relation between the specific capacitance and the current density for the electrochemically nitrogen-doped graphene electrodes measured in 1 M NaCl solution. It is worth mentioning here that the specific capacitance of the ECNG is higher than that of any reported oxides-free rGO-based materials measured in the same electrolyte.

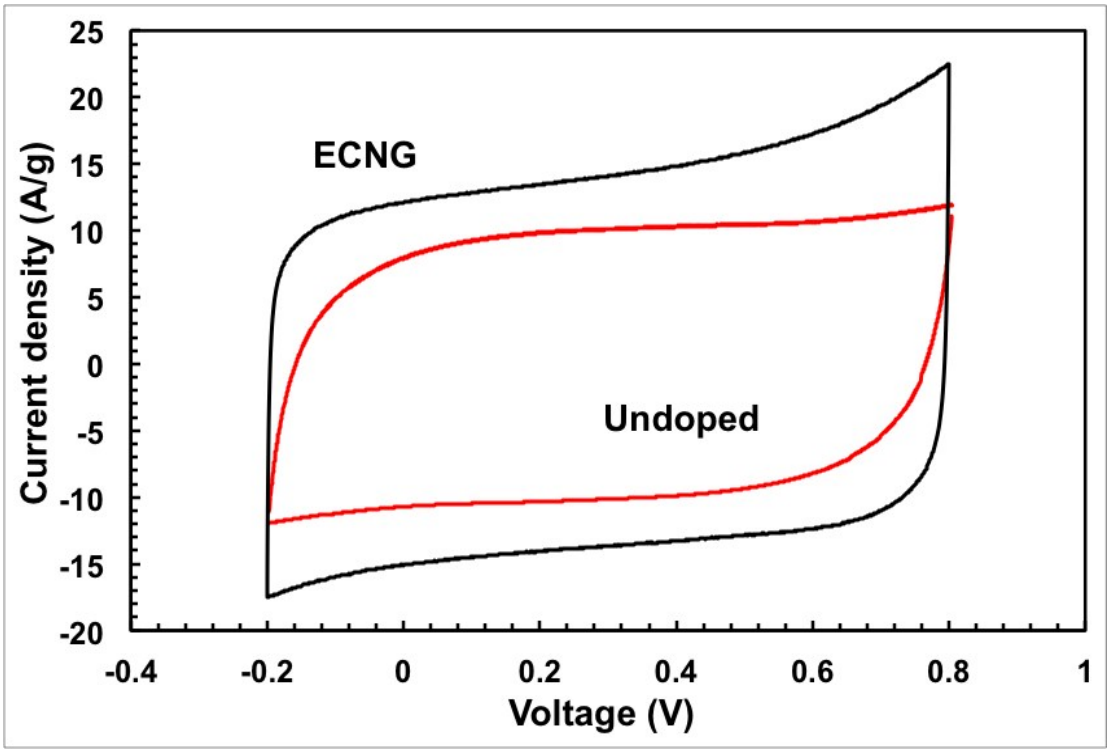

Figure S7: CV measured for the ECNG and the controlled undoped sample showing the effect of the doping on increasing the specific capacitance.

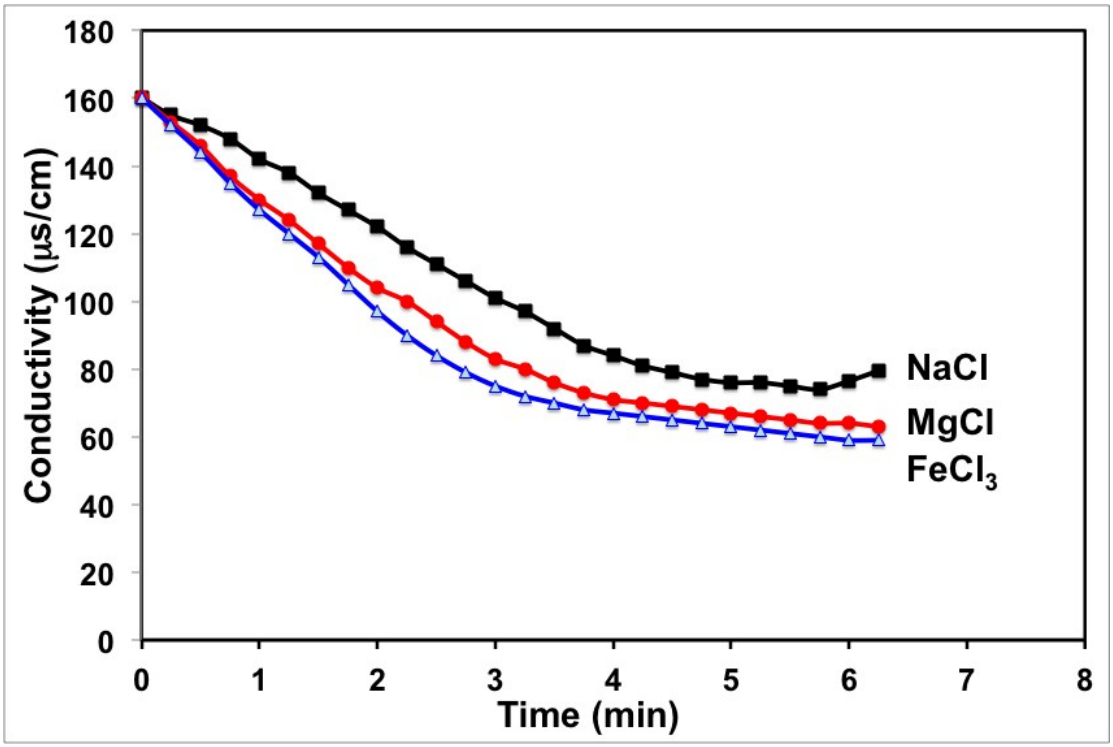

Figure S8: The change in the conductivity with time for the ECNG measured in different types of salts solution. The initial conductivity was kept constant for comparison.

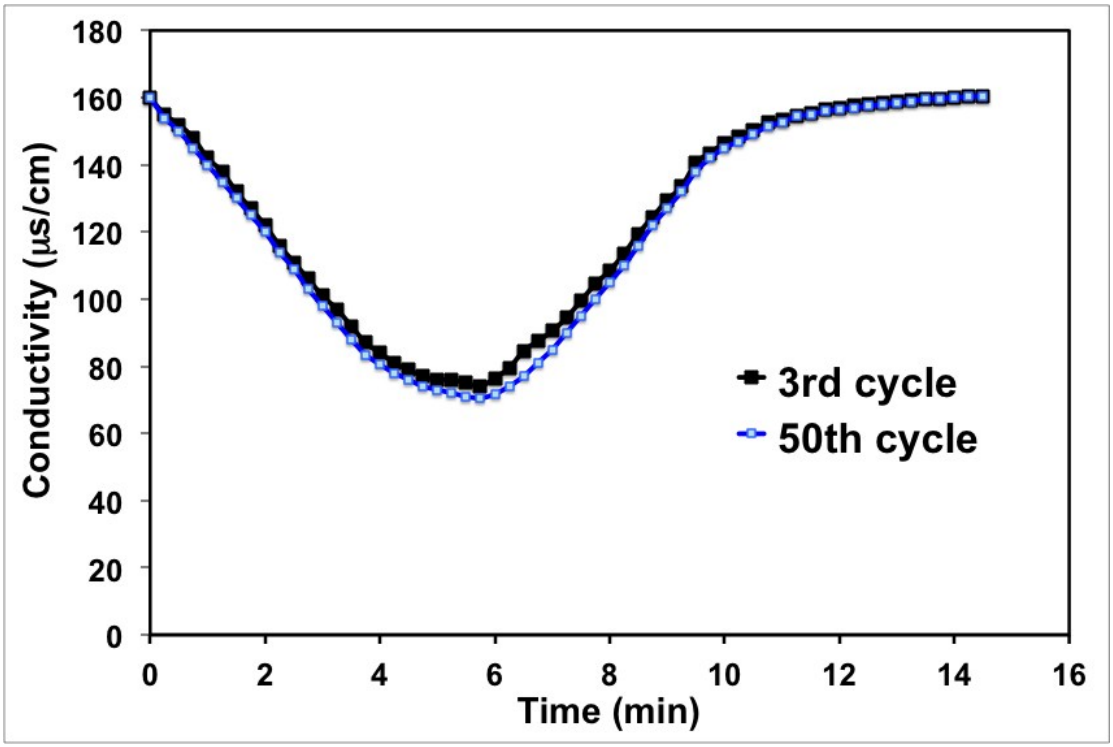

Figure S9: The conductivity curve of the ECNG electrode in the CDI device after 3 and 50 cycles, confirming the stability of the electrode.

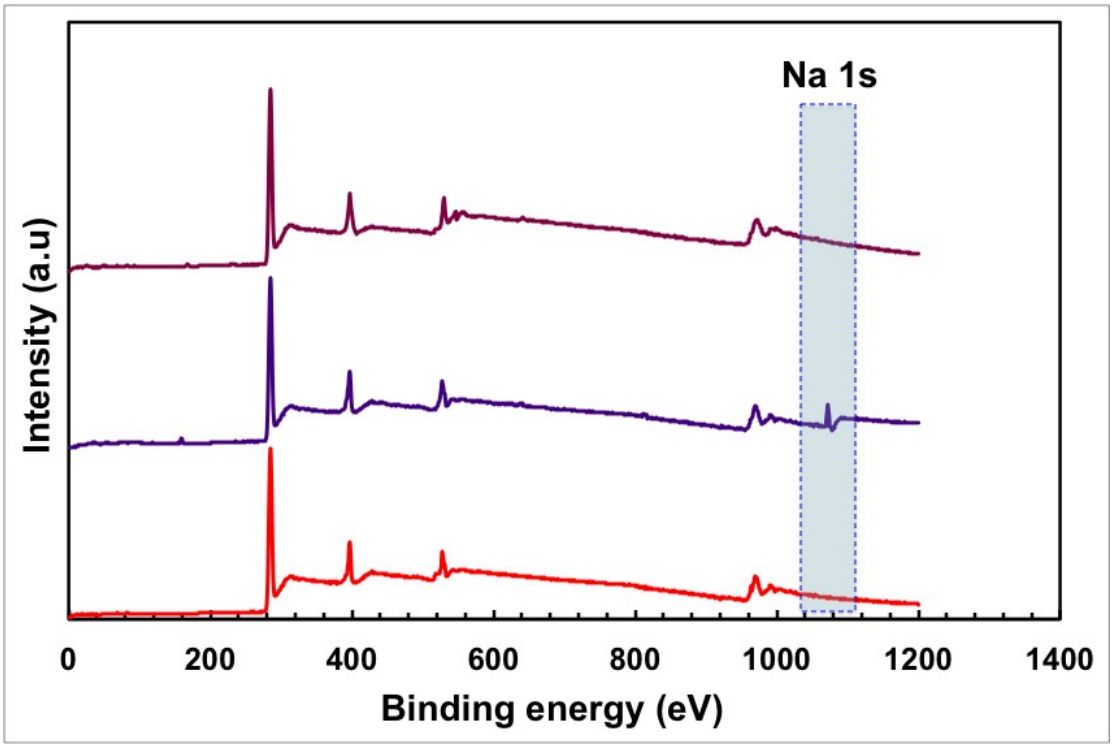

Figure S10: XPS spectra of ECNG before adsorption (red), after the adsorption of the 20th cycle (purple), and after the desorption of the 20th cycle (brown). The position of the Na s1 peak is highlighted.
The complete disappearance of the Na S1 peak after 20 desorption cycles of the clearly confirming the good reversibility of the adsorption/desorption process on the ECNG electrodes.

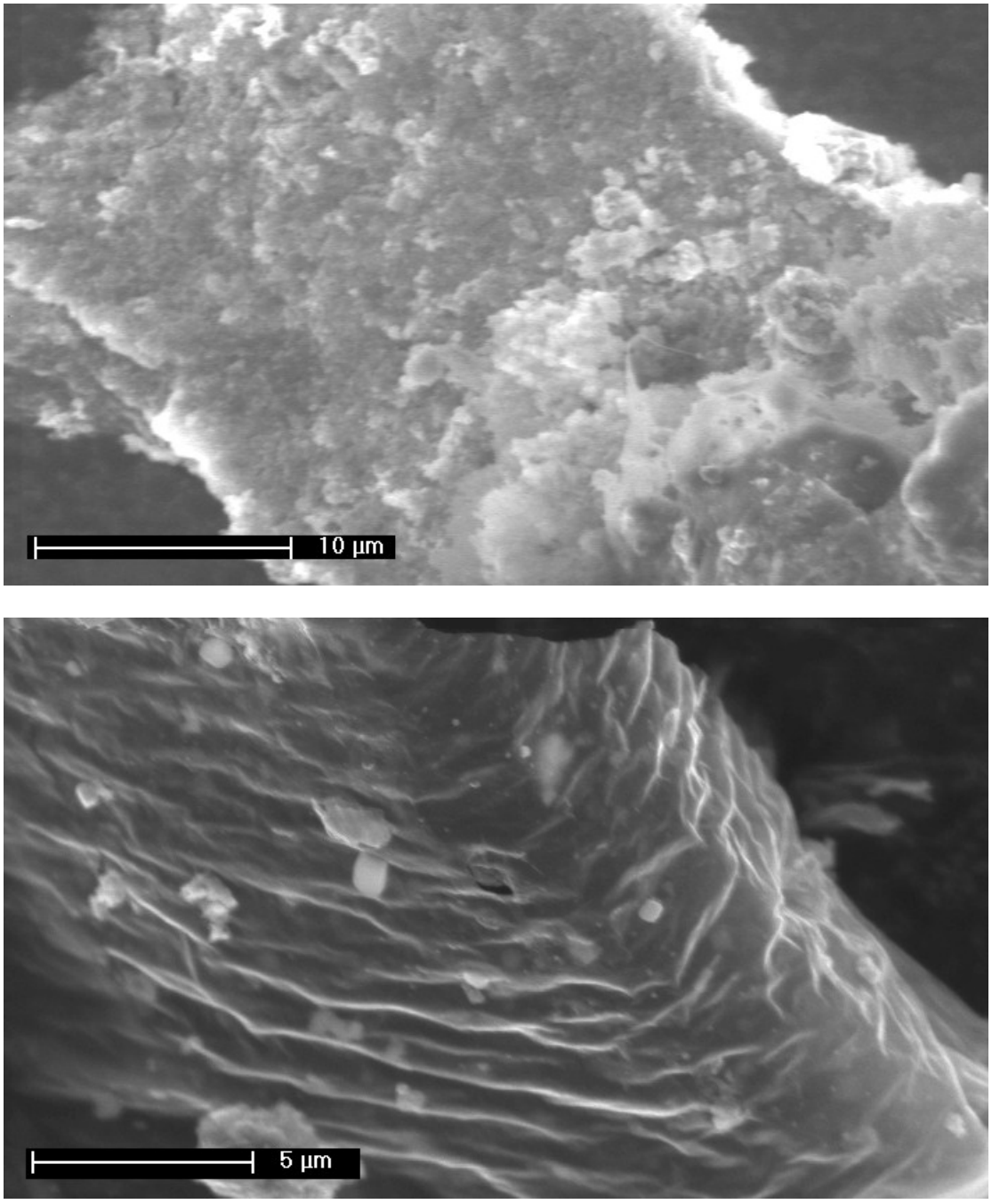

Figure S11: SEM images of the ECNG after the adsorption of the 20th cycle (top), and after the desorption of the same cycle (bottom). The wavy morphology of the ECNG is well maintained after cycling the electrode.

Table S2. Comparison of the electrochemical performance of rGO and N-doped rGO supercapacitor electrodes from different reduction method

Materials	Process	C/O ratio	Electrical conductivity (S/m)	Specific Capacitance (F/g)	Specific surface area (m^2/g)	Specific capacitance Retention %
Activated rGO	Reduction by microwave irradiation then activated by KOH [1]	35	500 (Pressed Powder)	200 ionic liquid	3100	97 after 10000 cycles
rGO	Reduction by hydrazine at 100 ^oC.[2]	11.5	200 (Pressed Powder)	135 KOH	705	Unknown
rGO	Reduction with Hydrazine vapor at low pressure.[3]	7.3	100 Film	205 KOH	320	90 after 1200 cycles
rGO	Solvothermal reduction in propylene carbonate at 150 ^oC.[4]	8.3	2100 (Paper-like)	120 Organic	Unknown	Unknown
rGO	Thermal reduction at 200 ^oC under high vacuum (below 1 Pa).[5]	10	Unknown	122 KOH	350	~ 94 after 100 cycles
rGO	Reduction with urea at 95 ^oC followed by annealing at 800 ^oC under nitrogen.[6]	19.7	4520 (Annealed paper)	172 H_2SO_4	630	94% after 1200 cycle
rGO	Reduction with hydrobromic acid at 110 ^oC.[7]	3.9	0.023	348 in H_2SO_4 and 158 in ionic liquid (pseudocapacitance involved)	Unknown	Increased to 125 % after 1800 cycle
rGO	Solvothermal reduction in DMF at 150 ^oC.[1]	5.97	Unknown	276 H_2SO_4 (pseudocapacitance involved)	Unknown	Increased to 106 % after 1980 cycles
rGO	Thermal reduction at 1050 ^oC.[8]	10[9]	2300 (Pressed powder)[9]	117 H_2SO_4	925	Unknown

rGO	Reduction with urea at 95 ^{o}C.[6]	4.5	43 (Paper-like)	255 H_2SO_4 (pseudocapacitance involved)	590	93% after 1200 cycles
rGO	Hydrothermal reduction with sodium ascorbate at 95 ^{o}C.[10]	10.3	1 (hydrogel)	190 H_2SO_4[11] 186 solid state	414	93.6 after 10000 cycles
rGO	Electrochemical reduction in molten salt.[12]	12.5	2300 (membrane)	255 KOH	565	95% after 5000 cycles
rGO	Reduction by laser irradiation.[13]		1738 (film)	204 solid state	1520	95% after 1000 cycles
rGO	Reduction by Li in molten LiCl-KCl at 370 ^{o}C.[14]	7	2400 (paper-like)	203 KOH	320	97% after 2000 cycles
N-doped graphene hydrogels	Hydrothermal Process [15]	~8		190.1 KOH		94% after 4000 cycles
Crumpled N-doped graphene	Polymerisation and heating in Ar at 900 ^{o}C [16]	~4		302 KOH	490	96.1% after 5000
N-doped graphene hydrogels	Hydrothermal reduction and functionalization with formamide [17]			275 KOH	665	
N-doped graphene	Hydrothermal Process	5.4		326 KOH	593	99.58% after 2000 cycle

Table S3. Salt electrosorption performance reported for different carbon materials as electrodes for CDI.

Carbon Materials	Initial Concentration (mg/ml)	Electrosorption capacity(mg/g)	Time until equilibrium (min)	Electrosorption rate(mg/g.min)	Charge efficiency	Flow rate (mL/min)	Cell potential (V)	Ref
Activated Carbon	1000	5.9	~7		0.53	3	1.6	[18]
Graphene xerogels – chitosan-Mn3O4	300	12.7	90			10	1.6	[19]
rGO/activated carbon	50	0.8	~60	0.12	0.24	25	2	[20]
Activated Carbon/QPVP	500	20.6	~10	1	0.68	8.67	1.2	[21]
Carbon beads		11.5		0.104	0.80	22	1.2	[22]
Activated carbon cloth/ZnO	1000	7.7	~6		0.78	3	1.6	[18]
Amine Modified Microporous Carbon	250	5.3	~60		0.53	20	1.1	[23]
Graphene-Fe3O4	300	10.3	100			10	1.6	[24]
Amine and carboxylic group modified graphene	300	18.43	~10		0.87	20	1.4	[25]
Sulfonic and amine functionalised graphene	500	13.72	~80	0.12	0.85	40	1.4	[26]
Activated graphene	86	14.25	~7	2.01	0.83	10	1.8	[27]
Graphene-like nanoflakes	25	1.3	> 40			45	2	[28]
Graphene-CNT	29	1.4	~120			25	2	[29]

Graphene aerogel/TiO_2	500	15.1	~6		0.68	30	1.2	[30]
Activated 3D graphene	70	11.86	~25			10	2	[31]
Cellulose Derived Graphenic Fibers	500	13.1	~90-120				1.2	[32]
Sulfonated graphene- carbon nanofibers	100	9.54	~65		0.43	5	1.6	[33]
Graphene-coated carbon spheres	29	2.3	~120			25	1.6	[34]
Sponge templated graphene	52	4.95	~60			3	1.5	[35]
Porous Carbon Rods	1000	16.2	~40			27	1.2	[36]
3-D macroporous graphene	52	5.93	~50			25	2	[37]

The equilibrium is defined as the point where the conductivity of the outlet stream stopped decreasing and started to increase.

References

1. Lin, Z., et al., *Superior Capacitance of Functionalized Graphene.* The Journal of Physical Chemistry C, 2011. **115**(14): p. 7120-7125.
2. Stoller, M.D., et al., *Graphene-Based ultracapacitors.* Nano Letters, 2008. **8**(10): p. 3498-3502.
3. !!! INVALID CITATION !!! [3].
4. !!! INVALID CITATION !!! [4].
5. !!! INVALID CITATION !!! [5].
6. Lei, Z., L. Lu, and X.S. Zhao, *The Electrocapacitive Properties of Graphene Oxide Reduced by Urea.* Energy & Environmental Science, 2012. **5**(4): p. 6391-6399.
7. Chen, Y., et al., *High Performance Supercapacitors Based on Reduced Graphene Oxide in Aqueous and Ionic Liquid Electrolytes.* Carbon, 2011. **49**(2): p. 573-580.
8. !!! INVALID CITATION !!! [8].
9. Schniepp, H.C., et al., *Functionalized Single Graphene Sheets Derived from Splitting Graphite Oxide.* The Journal of Physical Chemistry B, 2006. **110**(17): p. 8535-8539.
10. Sheng, K.-x., et al., *High-Performance Self-Assembled Graphene Hydrogels Prepared by Chemical Reduction of Graphene Oxide.* New Carbon Materials, 2011. **26**(1): p. 9-15.
11. Xu, Y., et al., *Flexible Solid-State Supercapacitors Based on Three-Dimensional Graphene Hydrogel Films.* ACS Nano, 2013. **7**(5): p. 4042-4049.
12. Abdelkader, A.M., *Electrochemical synthesis of highly corrugated graphene sheets for high performance supercapacitors.* Journal of Materials Chemistry A, 2015. **3**(16): p. 8519-8525.
13. El-Kady, M.F., et al., *Laser Scribing of High-Performance and Flexible Graphene-Based Electrochemical Capacitors.* Science, 2012. **335**(6074): p. 1326-1330.
14. Abdelkader, A.M., et al., *Alkali reduction of graphene oxide in molten halide salts: Production of corrugated graphene derivatives for high-performance supercapacitors.* ACS Nano, 2014. **8**(11): p. 11225-11233.
15. Chen, P., et al., *Hydrothermal synthesis of macroscopic nitrogen-doped graphene hydrogels for ultrafast supercapacitor.* Nano Energy, 2013. **2**(2): p. 249-256.
16. Wen, Z., et al., *Crumpled Nitrogen-Doped Graphene Nanosheets with Ultrahigh Pore Volume for High-Performance Supercapacitor.* Advanced Materials, 2012. **24**(41): p. 5610-5616.
17. Wang, Y., et al., *Generation of three dimensional pore-controlled nitrogen-doped graphene hydrogels for high-performance supercapacitors by employing formamide as the modulator.* Journal of Materials Chemistry A, 2017. **5**(4): p. 1442-1445.
18. Laxman, K., et al., *Improved desalination by zinc oxide nanorod induced electric field enhancement in capacitive deionization of brackish water.* Desalination, 2015. **359**: p. 64-70.
19. !!! INVALID CITATION !!! [19].

20. Li, H., et al., *Reduced graphene oxide and activated carbon composites for capacitive deionization.* Journal of Materials Chemistry, 2012. **22**(31): p. 15556-15561.
21. Wu, T., et al., *Surface-treated carbon electrodes with modified potential of zero charge for capacitive deionization.* Water Research, 2016. **93**: p. 30-37.
22. Krüner, B., et al., *Hydrogen-treated, sub-micrometer carbon beads for fast capacitive deionization with high performance stability.* Carbon, 2017. **117**: p. 46-54.
23. Gao, X., et al., *Enhanced Salt Removal in an Inverted Capacitive Deionization Cell Using Amine Modified Microporous Carbon Cathodes.* Environmental Science & Technology, 2015. **49**(18): p. 10920-10926.
24. Gu, X., et al., *Fabrication of mesoporous graphene electrodes with enhanced capacitive deionization.* Electrochimica Acta, 2015. **182**: p. 183-191.
25. El-Deen, A.G., et al., *Flexible 3D Nanoporous Graphene for Desalination and Bio-decontamination of Brackish Water via Asymmetric Capacitive Deionization.* ACS Applied Materials & Interfaces, 2016. **8**(38): p. 25313-25325.
26. Liu, P., et al., *Grafting sulfonic and amine functional groups on 3D graphene for improved capacitive deionization.* Journal of Materials Chemistry A, 2016. **4**(14): p. 5303-5313.
27. Zoromba, M.S., et al., *Electrochemical Activation of Graphene at Low Temperature: The Synthesis of Three-Dimensional Nanoarchitectures for High Performance Supercapacitors and Capacitive Deionization.* ACS Sustainable Chemistry & Engineering, 2017.
28. Li, H., et al., *Novel Graphene-Like Electrodes for Capacitive Deionization.* Environmental Science & Technology, 2010. **44**(22): p. 8692-8697.
29. Zhang, D., et al., *Enhanced capacitive deionization performance of graphene/carbon nanotube composites.* Journal of Materials Chemistry, 2012. **22**(29): p. 14696-14704.
30. Yin, H., et al., *Three-Dimensional Graphene/Metal Oxide Nanoparticle Hybrids for High-Performance Capacitive Deionization of Saline Water.* Advanced Materials, 2013. **25**(43): p. 6270-6276.
31. Li, Z., et al., *3D porous graphene with ultrahigh surface area for microscale capacitive deionization.* Nano Energy, 2015. **11**: p. 711-718.
32. Pugazhenthiran, N., et al., *Cellulose Derived Graphenic Fibers for Capacitive Desalination of Brackish Water.* ACS Applied Materials & Interfaces, 2015. **7**(36): p. 20156-20163.
33. Qian, B., et al., *Sulfonated Graphene as Cation-Selective Coating: A New Strategy for High-Performance Membrane Capacitive Deionization.* Advanced Materials Interfaces, 2015. **2**(16): p. 1500372-n/a.
34. Wang, H., et al., *Design of graphene-coated hollow mesoporous carbon spheres as high performance electrodes for capacitive deionization.* Journal of Materials Chemistry A, 2014. **2**(13): p. 4739-4750.
35. Yang, Z.Y., et al., *Sponge-templated preparation of high surface area graphene with ultrahigh capacitive deionization performance.* Advanced Functional Materials, 2014. **24**(25): p. 3917-3925.

36. Xu, X., et al., *Shuttle-like Porous Carbon Rods from Carbonized Metal–Organic Frameworks for High-Performance Capacitive Deionization.* ChemElectroChem, 2016. **3**(6): p. 993-998.
37. Wang, H., et al., *Three-dimensional macroporous graphene architectures as high performance electrodes for capacitive deionization.* Journal of Materials Chemistry A, 2013. **1**(38): p. 11778-11789.